AIAA JOURNAL
Vol. 34, No. 12, December 1996

Implicit Solution Method for Incompressible Navier–Stokes Equations Including Two-Layer k-τ Turbulence Model

Jürg Küffer,* Bernhard Müller,† and Torstein K. Fanneløp‡
Swiss Federal Institute of Technology, Zürich 8092, Switzerland

The two-dimensional incompressible Navier–Stokes equations including a low-Reynolds-number two-layer k-τ turbulence model are solved by an implicit time-stepping routine using the method of artificial compressibility. The two-layer model uses a transport equation for the turbulent kinetic energy k and a new algebraic relationship for the turbulent time scale τ near the wall but reverts to the two-equation k-τ turbulence model in the bulk of the flow away from the wall. The algebraic relationship for the turbulent time scale τ and the eddy-viscosity damping function f_μ are validated by direct numerical simulation data and asymptotic analysis of near-wall turbulence. A fifth-order upwind-biased differencing scheme is used to discretize the convective and pressure terms and second-order central differences are employed for other spatial derivatives. The nonlinear equations are solved using the preconditioned generalized minimal residual technique in conjunction with numerical linearization. A $LD^{-1}U$ factorization of the approximate Jacobian matrix is used as preconditioning matrix. The iterative scheme has good vectorization properties and runs at about 160 Mflops on one processor of a Cray Y-MP. The results for turbulent channel flows at low Reynolds numbers are in good agreement with direct numerical simulation data even in the viscous sublayer. Compared with experimental data, the simulation of the turbulent flow over a backward-facing step in a parallel and a diverging channel shows a better agreement for the reattachment length than comparable two-equation models.

Introduction

CHORIN'S[1] method of artificial compressibility has often been used to solve the incompressible Navier–Stokes equations. Recently, Rogers and Kwak[2] presented a solution method combining Chorin's scheme with an accurate upwind differencing scheme and an efficient implicit time-stepping routine. The goal of our work is to extend the solution method for the continuity and momentum equations to include a two-equation low-Reynolds-number turbulence model.

A good overview of several low-Reynolds-number two-equation turbulence models can be found in Refs. 3 and 4. Detailed comparisons of different low-Reynolds-number turbulence model computations and direct numerical simulation (DNS) data are presented in Refs. 5–8. The problem of predicting adverse pressure flows accurately is discussed in Refs. 9–11. For the present work we have chosen the low-Reynolds-number k-τ turbulence model developed by Speziale et al.[4] On solid walls the model has the advantage of a natural boundary condition for the turbulent time scale $\tau \equiv k/\varepsilon$ (where k is the turbulent kinetic energy and ε is the turbulent dissipation rate). Thangam et al.[12] have reported good results for test cases with strong adverse pressure gradients. However, in our numerical tests we experienced several problems with the transport equation of the turbulent time scale τ in the immediate vicinity of walls. The turbulent time scale tended to small or even negative values and destabilized the computations. This unphysical behavior was especially dominant in the corner region of the backward-facing step. To overcome this problem we stabilized the near-wall behavior of the turbulent time scale by a new algebraic model to be used only in the vicinity of walls. This algebraic model is based on the Norris–Reynolds[13] length scale and has to be matched with the transport equation somewhere inside the wall layer. This approach is an alternative to the method of Rodi[14] and Cordes,[15] which combines a one-equation model for the wall region with a standard high-Reynolds-number k-ε model for the bulk of the flow.

Traditional implicit techniques solve the algebraic system of linearized equations based on the analytically derived Jacobian matrix. To derive this Jacobian matrix analytically, several approximations are necessary. For example, when turbulence models are used, the eddy viscosity has to be frozen at the latest known time level. Such approximations often lead to restrictions of the Courant–Friedrichs–Lewy (CFL) number. This can be avoided by numerical linearization of the nonlinear equations using the generalized minimal residual (GMRES) technique by Saad and Schultz[16] in conjunction with a finite difference quotient.[17,18] With this it becomes possible to solve the nonlinear equations directly without a restriction of the CFL number. As shown by Ajmani et al.[19] and Venkatakrishnan and Mavriplis,[20] the efficiency of GMRES can be improved dramatically by a good preconditioning. Most authors use the incomplete lower-upper decomposition (ILU) of the Jacobian matrix as a preconditioning matrix. This method has the drawback of poor vectorization properties and is therefore not optimal for a vector computer. A much better preconditioning can be realized with the $LD^{-1}U$ factorization of an approximate Jacobian matrix. This factorization is similar to the lower-upper symmetric-Gauss–Seidel algorithm by Yoon and Jameson,[21] Yoon et al.,[22] and Yoon and Kwak.[23] The combination of all of these techniques results in an efficient method for solving nonlinear systems of equations.

The two-layer k-τ turbulence model and the iterative solution technique have been tested by computing the fully turbulent channel flow at low Reynolds numbers and the turbulent flow over a backward-facing step at a high Reynolds number. The results of the channel computations are compared with DNS data by Hirschberg[24] and Kim (see Ref. 25) and show good agreement. Driver and Seegmiller[26] have presented measurements for two configurations of the backward-facing step flow. In both cases, good results have been obtained by the present two-layer k-τ turbulence model.

In the following sections, a new algebraic model for the turbulent time scale and a new damping function for the eddy viscosity are derived. Once the governing equations are established, the spatial discretization and the implicit time-stepping scheme, including the preconditioned GMRES technique, are discussed. Finally, the

Received Jan. 30, 1996; revision received July 25, 1996; accepted for publication July 26, 1996; also published in *AIAA Journal on Disc*, Volume 2, Number 1.

*Research Scientist, Institute of Fluid Dynamics, Sonneggstrasse 3.
†Professor, Institute of Fluid Dynamics, Sonneggstrasse 3.
‡Professor and Head, Institute of Fluid Dynamics, Sonneggstrasse 3. Member AIAA.

computed results for the turbulent channel flow and the turbulent flow over a backward-facing step are presented and relevant comparisons are made.

Two-Layer k-τ Turbulence Model

From the Norris–Reynolds[13] one-equation model, one can derive an algebraic model for the turbulent time scale τ_{NR},

$$\tau_{NR} = \frac{k}{\varepsilon} = \frac{y_w^2}{c_\tau \sqrt{k} y_w + 2\nu} \tag{1}$$

where y_w is the normal distance to the wall, ν is the kinematic viscosity, and $c_\tau = 0.401$ is a constant, chosen to fit the correct behavior in the logarithmic layer. Moreover, the turbulent time scale has the correct asymptotic bahavior in the viscous sublayer ($\tau^+ = y^{+2}/2$) and in the logarithmic layer ($\tau^+ = \kappa y^+/\sqrt{C_\mu}$). The variables $\tau^+ = \tau u_\tau^2/\nu$ and $y^+ = y_w u_\tau/\nu$ are nondimensionalized by the friction velocity u_τ and the kinematic viscosity ν. The constants are $\kappa = 0.41$ (von Kármán) and $C_\mu = 0.09$.

Although the algebraic model τ_{NR} has the correct asymptotic behavior close to the wall and in the logarithmic layer, it is not very accurate in the buffer layer (see Fig. 1). This can be corrected by using data from DNS. Two sets of DNS data for plane channel flow at Reynolds numbers $Re_\tau = 1.8 \times 10^2$ (Ref. 24) and $Re_\tau = 3.95 \times 10^2$ [Kim (see Ref. 25)] have been used. The Reynolds number $Re_\tau \equiv u_\tau h/\nu$ is based on the friction velocity u_τ and the channel half-width h. The comparison with the DNS data suggests the introduction of a damping term, which corrects the behavior of the turbulent time scale in the buffer layer. This additional damping term is based on the ratio of the eddy viscosity ν_T and the kinematic viscosity ν. The constant $c_{\tau\nu}$ can be determined from the comparison with the DNS data; we find $c_{\tau\nu} = 12.0$,

$$\tau_{\text{alg}} = \frac{y_w^2}{c_\tau \sqrt{k} y_w \sqrt{\tanh(\nu_T/c_{\tau\nu}\nu)} + 2\nu} \tag{2}$$

The algebraic model for the turbulent time scale shows good agreement with the DNS data only in the vicinity of the wall (Fig. 1). In this region, the algebraic model τ_{alg} will be used for the computations. As the wall distance increases ($y^+ > 30$), a blending between the algebraic model τ_{alg} and the transport equation for the turbulent time scale τ_{pde} will be used. In the logarithmic layer and in the bulk of the flow, only the transport equation for the turbulent time scale will be used to obtain the solution.

For the k-τ turbulence model[4] the eddy viscosity ν_T is determined by

$$\nu_T = C_\mu f_\mu k \tau \tag{3}$$

with $C_\mu = 0.09$. Here, a new damping function f_μ for the eddy viscosity is introduced. This damping function [Eq. (4)] is based on the turbulent Reynolds numbers $R_y \equiv \sqrt{(k)} y_w/\nu$ and $R_T \equiv k\tau/\nu$ and is valid in the whole flowfield, including the viscous sublayer

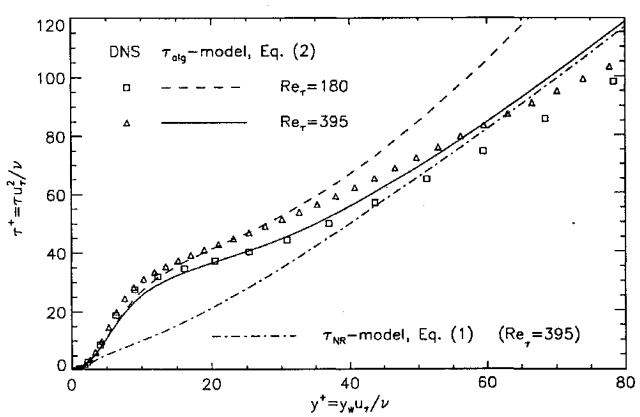

Fig. 1 Comparison of two algebraic models for the turbulent time scale τ with DNS data.

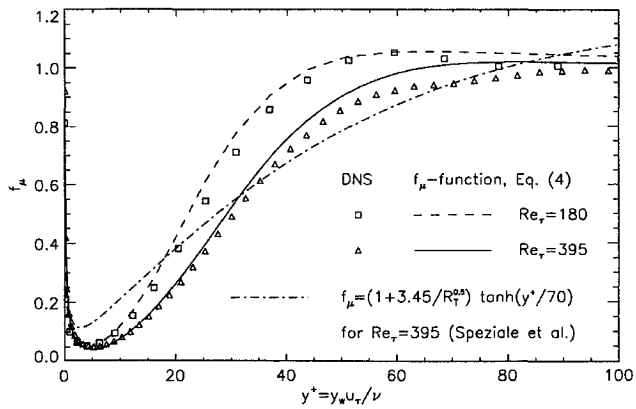

Fig. 2 DNS data compared with two damping functions f_μ.

and the logarithmic layer. From the comparison with the DNS data, the constants are evaluated as $c_{f1} = 33.0$ and $c_{f2} = 75.0$,

$$f_\mu = \frac{\tanh\left[\left(R_y^2/c_{f1}R_T\right)^{1.5}\right]}{\sqrt{\tanh(R_y/c_{f2})}} \tag{4}$$

The new damping function shows better agreement with the DNS data than the function proposed by Speziale et al.[4] (Fig. 2). The function proposed here has, moreover, the correct asymptotic behavior close to the wall ($f_\mu \sim 1/y^+$) and in the logarithmic layer ($f_\mu = 1$).

A major advantage of the new turbulent time scale model and the new damping function is the fact that the friction velocity u_τ is not a parameter of these models. The terms τ_{alg} and f_μ avoid the problem of determining the friction velocity in complex flows. Therefore, replacing the transport equation for τ by the algebraic relation τ_{alg} near walls considerably improves the robustness of the k-τ turbulence model.

Governing Equations

The two-dimensional incompressible Navier–Stokes equations, including the two-layer k-τ turbulence model, are solved using the method of artificial compressibility. The equations are written in conservative form, with the density absorbed in the pressure term. Generalized coordinates are used in the form $\xi = \xi(x, y)$ and $\eta = \eta(x, y)$, which results in the following equation:

$$\frac{\partial \hat{\boldsymbol{Q}}}{\partial t} + \frac{\partial}{\partial \xi}(\hat{\boldsymbol{E}} - \hat{\boldsymbol{E}}_v) + \frac{\partial}{\partial \eta}(\hat{\boldsymbol{F}} - \hat{\boldsymbol{F}}_v) + \hat{\boldsymbol{H}} = 0 \tag{5}$$

where $\boldsymbol{Q}$ is the vector with the unknown pressure p (including the density), velocity components u and v, turbulent kinetic energy k, and the turbulent time scale τ,

$$\hat{\boldsymbol{Q}} = \hat{\boldsymbol{Q}}/J = (1/J)[p \quad u \quad v \quad k \quad \tau]^T \tag{6}$$

where J is the Jacobian determinant of the transformation. The terms $\hat{\boldsymbol{E}}$ and $\hat{\boldsymbol{F}}$ are the flux vectors, which are given by

$$\hat{\boldsymbol{E}} = \frac{1}{J}\begin{bmatrix} \beta U \\ \xi_x p + uU \\ \xi_y p + vU \\ kU \\ \tau U \end{bmatrix} \qquad \hat{\boldsymbol{F}} = \frac{1}{J}\begin{bmatrix} \beta V \\ \eta_x p + uV \\ \eta_y p + vV \\ kV \\ \tau V \end{bmatrix}$$

where β is the artificial compressibility parameter and $U = \xi_x u + \xi_y v$ and $V = \eta_x u + \eta_y v$ are the contravariant velocity components. The metrics of the transformation are represented by $\partial\xi/\partial x = \xi_x$,

etc. The diffusive fluxes $\hat{E}_v$ and $\hat{F}_v$ are derived assuming an orthogonal grid

$$\hat{E}_v = \frac{1}{J}\begin{bmatrix} 0 \\ \nu(\xi_x^2+\xi_y^2)u_\xi + \xi_x\tau_{xx} + \xi_y\tau_{xy} \\ \nu(\xi_x^2+\xi_y^2)v_\xi + \xi_x\tau_{yx} + \xi_y\tau_{yy} \\ (\nu+\nu_T/\sigma_k)(\xi_x^2+\xi_y^2)k_\xi \\ (\nu+\nu_T/\sigma_{\tau 2})(\xi_x^2+\xi_y^2)\tau_\xi \end{bmatrix} \tag{7}$$

$$\hat{F}_v = \frac{1}{J}\begin{bmatrix} 0 \\ \nu(\eta_x^2+\eta_y^2)u_\eta + \eta_x\tau_{xx} + \eta_y\tau_{xy} \\ \nu(\eta_x^2+\eta_y^2)v_\eta + \eta_x\tau_{yx} + \eta_y\tau_{yy} \\ (\nu+\nu_T/\sigma_k)(\eta_x^2+\eta_y^2)k_\eta \\ (\nu+\nu_T/\sigma_{\tau 2})(\eta_x^2+\eta_y^2)\tau_\eta \end{bmatrix}$$

where u_ξ, u_η, etc., are the velocity gradients and the turbulent stresses τ_{xy}, etc., are given by

$$\tau_{xx} = 2\nu_T(\xi_x u_\xi + \eta_x u_\eta) - \tfrac{2}{3}k \qquad \tau_{yy} = 2\nu_T(\xi_y v_\xi + \eta_y v_\eta) - \tfrac{2}{3}k \tag{8}$$

$$\tau_{xy} = \tau_{yx} = \nu_T(\xi_y u_\xi + \eta_y u_\eta + \xi_x v_\xi + \eta_x v_\eta)$$

All other terms arising from the turbulence model are collected in the source term vector $\hat{H}$,

$$\hat{H} = \frac{1}{J}\begin{bmatrix} 0 \\ 0 \\ 0 \\ k/\tau^{(\mathrm{av})} - P_k \\ 1 - C_{\varepsilon 2}f_2 - (1-C_{\varepsilon 1})P_k\tau/k^{(\mathrm{av})} - D \end{bmatrix} \tag{9}$$

with the production of the turbulent kinetic energy P_k,

$$P_k = \tau_{xx}(\xi_x u_\xi + \eta_x u_\eta) + \tau_{yy}(\xi_y v_\xi + \eta_y v_\eta) + \tau_{xy}(\xi_y u_\xi + \eta_y u_\eta + \xi_x v_\xi + \eta_x v_\eta) \tag{10}$$

the damping function f_2

$$f_2 = 1 - 0.222e^{-R_T^2/36} \tag{11}$$

and the additional term D

$$D = \frac{2}{k^{(\mathrm{av})}}\left(\nu + \frac{\nu_T}{\sigma_{\tau 1}}\right)\left[(\xi_x^2+\xi_y^2)k_\xi\tau_\xi + (\eta_x^2+\eta_y^2)k_\eta\tau_\eta\right] - \frac{2}{\tau^{(\mathrm{av})}}\left(\nu + \frac{\nu_T}{\sigma_{\tau 2}}\right)\left[(\xi_x^2+\xi_y^2)\tau_\xi^2 + (\eta_x^2+\eta_y^2)\tau_\eta^2\right] \tag{12}$$

To get a numerically robust scheme it has been necessary to average some source terms. Those are indicated by the superscript av. At the grid point with indices (i, j) the variable ϕ is averaged by

$$\phi_{i,j}^{(\mathrm{av})} = \tfrac{1}{8}(4\phi_{i,j} + \phi_{i+1,j} + \phi_{i-1,j} + \phi_{i,j+1} + \phi_{i,j-1})$$

The eddy viscosity ν_T is given by Eq. (3), and near a solid wall, the eddy viscosity is damped by the damping function, Eq. (4). In the vicinity of a solid wall, the algebraic model for the turbulent time scale τ_{alg} [Eq. (2)] is used instead of the transport equation. The blending between the algebraic model τ_{alg} and the transport equation τ_{pde} is based on the ratio of the eddy viscosity and the laminar viscosity and is performed by the following function:

$$\tau = \omega_\tau\tau_{pde} + (1-\omega_\tau)\tau_{\mathrm{alg}}$$

with

$$\omega_\tau = \frac{1}{2}\left[1 + \tanh\left(\frac{\nu_T/\nu - c_{\nu 1}}{c_{\nu 0}}\right)\right] \tag{13}$$

The constants used in the turbulence model are listed in Table 1.

Table 1 Constants of the low-Reynolds-number two-layer k-τ turbulence model

C_μ	$C_{\varepsilon 1}$	$C_{\varepsilon 2}$	σ_k	$\sigma_{\tau 1}$	$\sigma_{\tau 2}$	c_τ	$c_{\tau\nu}$	c_{f1}	c_{f2}	$c_{\nu 0}$	$c_{\nu 1}$
0.09	1.44	1.833	1.2	1.36	1.36	0.401	12.0	33.0	75.0	3.0	10.0

Spatial Discretization

The system of equations is discretized by a finite difference method. The fifth-order upwind-biased differencing scheme of Rogers and Kwak[2] (also see Ref. 27), based on flux-difference splitting, is used to compute the convective fluxes. The Jacobian matrices of the flux vectors and the related matrices with the eigenvectors have been extended to fit the governings equations, including the turbulence model. The details of this formulation are given in Küffer.[28] The fifth-order upwind scheme has the advantage of suppressing oscillations by adding a minimal amount of physically based dissipation. For the viscous terms and the first derivatives in the turbulence model, a second-order central difference formula is applied.

Implicit Time-Stepping Scheme

For stiff problems, which frequently arise in computational fluid dynamics, the convergence rate of an explicit method degrades rapidly, resulting in an inefficient solution technique. To speed up the convergence, an implicit method is required.

In general, the Navier–Stokes equations, including the turbulence model and the boundary conditions, can be written as a function $\hat{G}(Q)$,

$$\hat{G}(Q) = \frac{\partial\hat{Q}}{\partial t} - \hat{R}(Q) = 0 \tag{14}$$

where $\hat{R}(Q)$ represents the spatial terms of the Navier–Stokes equations. The usual way to get an implicit time-stepping scheme is the linearization of $\hat{R}(Q)$ at the latest known time level n. Using the implicit Euler scheme, we obtain

$$\left[\frac{I}{J\Delta t} - \frac{\partial\hat{R}}{\partial Q}\right]^n \Delta Q = \hat{R}(Q^n) \tag{15}$$

with the solution vector $\Delta Q = Q^{n+1} - Q^n$. The term in square brackets is the Jacobian matrix $(\partial\hat{G}/\partial Q)^n$. To construct this Jacobian matrix analytically, several approximations are necessary. To save computer storage and to guarantee block-diagonal dominance of the Jacobian matrix, one has to approximate the fifth-order upwind scheme used in $\hat{R}(Q)$ by a first-order scheme in $\partial\hat{R}/\partial Q$. Furthermore, when using turbulence models, quantities such as the eddy viscosity have to be frozen at the time level n. However, these approximations of the Jacobian matrix have a negative influence on the stability of the implicit time-stepping scheme.

Alternatively one can use a numerical linearization to compute the Jacobian matrix. Or even better, one uses the GMRES solution method and replaces the matrix-vector product by a finite difference quotient. With this numerical linearization, the stability of the implicit time-stepping scheme is maintained up to high CFL numbers.

GMRES

GMRES, developed by Saad and Schultz,[16] is an iterative solution method for solving nonsymmetric linear systems. At each time step, one starts from an approximate solution ΔQ_0 of Eq. (15). GMRES forms an orthogonal basis $v_1, \ldots, v_k$ (termed search directions), spanning the Krylov subspace, and finds the best possible solution for ΔQ_k by solving a minimization problem. The new ΔQ_k is a better estimate for the solution of Eq. (15). To reach the steady state as fast as possible, at every time step, one solves Eq. (15) only to a certain accuracy r,

$$r = \frac{\|\hat{R} - \hat{G}'\cdot\Delta Q_k\|_2}{\|\hat{R} - \hat{G}'\cdot\Delta Q_0\|_2}, \qquad \text{e.g.,} \qquad r \le 0.1 \tag{16}$$

The search vectors v_i have the same length as Eq. (15) has unknowns. As the number of GMRES iterations k increases, there is a tradeoff between the need for storage and the need for faster

convergence. Usually the number of GMRES iterations has to be limited to a maximum of between 20 and 40. If the accuracy ($r \leq 0.1$) cannot be achieved in these 20 and 40 iterations, the GMRES method can be restarted. In our test cases, restarting usually was not necessary.

Numerical Linearization

As indicated, GMRES does not really need the Jacobian matrix $\partial\hat{\boldsymbol{G}}/\partial\boldsymbol{Q}$ explicitly; it only needs the influence of a search vector $\boldsymbol{v}$ on the matrix $\partial\hat{\boldsymbol{G}}/\partial\boldsymbol{Q}$. Thus, the matrix-vector product can be replaced by a finite difference quotient.[17] Assuming we use the preconditioning matrix P, the numerical linearization reads as follows:

$$\frac{\partial\hat{\boldsymbol{G}}}{\partial\boldsymbol{Q}}\cdot\boldsymbol{P}^{-1}\cdot\boldsymbol{v}=\frac{\partial\hat{\boldsymbol{G}}}{\partial\boldsymbol{Q}}\cdot\boldsymbol{v}^{*}\approx\frac{\hat{\boldsymbol{G}}(\boldsymbol{Q}^{n}+\varepsilon^{*}\boldsymbol{v}^{*})-\hat{\boldsymbol{G}}(\boldsymbol{Q}^{n})}{\varepsilon^{*}} \tag{17}$$

where $\boldsymbol{v}^{*}=\boldsymbol{P}^{-1}\cdot\boldsymbol{v}$ and $\varepsilon^{*}=\varepsilon/\|\boldsymbol{v}^{*}\|_{2}$. On a Cray supercomputer with 64-bit arithmetic, the constant ε is chosen as 10^{-9}. With this numerical linearization it is now possible to solve the nonlinear system Eq. (14) directly. Therefore, the stability is maintained up to high CFL numbers.

Preconditioning

Unfortunately, the GMRES solution method is not very useful without a good preconditioner. Best convergence can be obtained if we use a preconditioning matrix $\boldsymbol{P}$ close to the Jacobian matrix $\partial\hat{\boldsymbol{G}}/\partial\boldsymbol{Q}$. Then the linear system including the right preconditioning takes the form

$$\left(\frac{\partial\hat{\boldsymbol{G}}}{\partial\boldsymbol{Q}}\right)^{n}\cdot\boldsymbol{P}^{-1}\cdot(\boldsymbol{P}\cdot\Delta\boldsymbol{Q})=\hat{\boldsymbol{R}}(\boldsymbol{Q}^{n}) \tag{18}$$

The so-called right preconditioning has the advantage that the right-hand side of Eq. (15) and the GMRES residual norm are not rescaled by the preconditioner. In Eq. (18), GMRES does not solve for the true solution vector $\Delta\boldsymbol{Q}$, but it solves for the product $\Delta\boldsymbol{Q}^{*}=\boldsymbol{P}\cdot\Delta\boldsymbol{Q}$. Therefore, at the end of the GMRES algorithm, the true solution vector has to be computed from

$$\Delta\boldsymbol{Q}=\boldsymbol{P}^{-1}\cdot\Delta\boldsymbol{Q}^{*} \tag{19}$$

The best suited preconditioner we found is the $\boldsymbol{LD}^{-1}\boldsymbol{U}$ factorization of an approximate Jacobian matrix $\tilde{\boldsymbol{G}}'$ of the exact Jacobian matrix $\hat{\boldsymbol{G}}'$,

$$\tilde{\boldsymbol{G}}'\approx\left(\frac{\partial\hat{\boldsymbol{G}}}{\partial\boldsymbol{Q}}\right)^{n} \tag{20}$$

This factorization is similar to the lower-upper symmetric-Gauss–Seidel algorithm by Yoon and Jameson,[21] Yoon et al.,[22] and Yoon and Kwak.[23] The term $\boldsymbol{D}$ denotes the main diagonal of the approximate Jacobian matrix $\tilde{\boldsymbol{G}}'$, and $\boldsymbol{L}$ and $\boldsymbol{U}$ denote the lower and upper triangular matrices including the diagonal $\boldsymbol{D}$. The elements in the row r and the column c of the matrices $\boldsymbol{L}$, $\boldsymbol{D}$, and $\boldsymbol{U}$ are defined as

$$\boldsymbol{D}_{(r,c)}=\tilde{\boldsymbol{G}}'_{(r,c)}\quad\text{for}\quad r=c\quad\text{and}\quad 0\quad\text{elsewhere}$$

$$\boldsymbol{L}_{(r,c)}=\tilde{\boldsymbol{G}}'_{(r,c)}\quad\text{for}\quad r\geq c\quad\text{and}\quad 0\quad\text{elsewhere}$$

$$\boldsymbol{U}_{(r,c)}=\tilde{\boldsymbol{G}}'_{(r,c)}\quad\text{for}\quad r\leq c\quad\text{and}\quad 0\quad\text{elsewhere}$$

The present $\boldsymbol{LD}^{-1}\boldsymbol{U}$ factorization differs from the one of Yoon et al. in that here $\boldsymbol{D}$ contains the diagonal elements and not the diagonal blocks. The following relation holds:

$$\tilde{\boldsymbol{G}}'=\boldsymbol{L}+\boldsymbol{U}-\boldsymbol{D}=\boldsymbol{LD}^{-1}\boldsymbol{U}+\boldsymbol{E} \tag{21}$$

and the factorization error $\boldsymbol{E}=-(\boldsymbol{L}-\boldsymbol{D})\boldsymbol{D}^{-1}(\boldsymbol{U}-\boldsymbol{D})$ can be dropped for the preconditioning. It is remarkable that the matrix elements of $\boldsymbol{L}$, $\boldsymbol{D}$, and $\boldsymbol{U}$ are the same as those of $\tilde{\boldsymbol{G}}'$. With this, no decomposition phase is necessary as is the case for the ILU preconditioning (incomplete LU factorization). Furthermore, the present factorization has the advantage of good vectorization properties on grid points with indices $i+j=\text{const}$ (i is the index for the ξ direction and j is the index for the η direction of the grid points in the computational domain). On one processor of the Cray Y-MP a performance of 160 Mflops was achieved with this factorization.

Approximate Jacobian Matrix

As a preconditioning matrix we use a factorization of an approximation of the Jacobian matrix $\partial\hat{\boldsymbol{G}}/\partial\boldsymbol{Q}$ of the nonlinear system Eq. (14). For the discretization used and the structured grid, the approximate Jacobian matrix $\tilde{\boldsymbol{G}}'$ is a banded matrix,

$$\tilde{\boldsymbol{G}}'_{i,j}=\text{banded matrix}\left[-\frac{\partial\hat{\boldsymbol{R}}_{i,j}}{\partial\boldsymbol{Q}_{i,j-1}},0,\ldots,0,-\frac{\partial\hat{\boldsymbol{R}}_{i,j}}{\partial\boldsymbol{Q}_{i-1,j}},\right.$$

$$\left.\frac{\boldsymbol{I}}{J_{i,j}\Delta t}-\frac{\partial\hat{\boldsymbol{R}}_{i,j}}{\partial\boldsymbol{Q}_{i,j}},-\frac{\partial\hat{\boldsymbol{R}}_{i,j}}{\partial\boldsymbol{Q}_{i+1,j}},0,\ldots,0,-\frac{\partial\hat{\boldsymbol{R}}_{i,j}}{\partial\boldsymbol{Q}_{i,j+1}}\right] \tag{22}$$

where i and j are the grid point indices for the ξ and η directions. Several approximations are necessary to construct the Jacobian matrix analytically. First, the fifth-order upwind scheme used on the right-hand side $\hat{\boldsymbol{R}}(\boldsymbol{Q})$ will be approximated by a first-order upwind scheme on the implicit side. Because of the smaller stencil, this saves computer memory. Moreover, the first-order upwind scheme guarantees the block-diagonal dominance of the Jacobian matrix $\tilde{\boldsymbol{G}}'$. At each grid point, the approximate Jacobian matrix $\tilde{\boldsymbol{G}}'$ forms 5×5 blocks. To estimate the diffusive terms the eddy viscosity is frozen at the latest time level. The source terms arising from the turbulence model are only retained on the implicit side if they improve the diagonal dominance of the approximate Jacobian matrix $\tilde{\boldsymbol{G}}'$. The detailed formulation of the approximate Jacobian matrix is given in Küffer.[28]

Local Time Stepping

For steady-state computations the method can be accelerated further by the use of local time steps. This is especially attractive when using low-Reynolds-number turbulence models with their rather small mesh sizes in the normal direction in the vicinity of solid walls. The local time step Δt can be computed from the following equation:

$$\Delta t=\frac{C_S}{\sqrt{\beta m}+4(\nu+C_\mu k\tau)m} \tag{23}$$

The term $m=\xi_x^2+\xi_y^2+\eta_x^2+\eta_y^2$ accounts for the local mesh sizes Δx and Δy ($\Delta\xi=\Delta\eta=1$). Assuming that the velocity squared u^2 is much smaller than the compressibility parameter β, one can approximate the artificial speed of sound $c=(u^2+\beta)^{0.5}$ by $c\approx\sqrt{\beta}$. The stability parameter C_S can be chosen between 1 and 100 or even higher, and it approximates the CFL number in the case of an inviscid flow.

Comparison of Different Solution Methods

The iterative GMRES solution method combined with the numerical linearization and the $\boldsymbol{LD}^{-1}\boldsymbol{U}$ preconditioning is compared with several other iterative methods. As a test case, the driven cavity flow at $Re=4\times10^{2}$ with 64×64 grid points has been chosen. For this laminar flow, the approximate Jacobian matrix $\tilde{\boldsymbol{G}}'$ can be computed and solved also without the aid of numerical linearization. The following solution methods are compared:

1) Line relaxation: solving $\tilde{\boldsymbol{G}}'\cdot\Delta\boldsymbol{Q}=\hat{\boldsymbol{R}}$ by several forward and backward sweeps in each coordinate direction similar to Rogers and Kwak.[2]

2) $LD^{-1}U$: solving $\boldsymbol{LD}^{-1}\boldsymbol{U}\cdot\Delta\boldsymbol{Q}=\hat{\boldsymbol{R}}$ directly.

3) GMRES/$\tilde{\boldsymbol{G}}'$/P=$LD^{-1}U$: solving $\tilde{\boldsymbol{G}}'\cdot\Delta\boldsymbol{Q}=\hat{\boldsymbol{R}}$ with $\boldsymbol{LD}^{-1}\boldsymbol{U}$ preconditioning (without numerical linearization).

4) GMRES/NumLin/P=$LD^{-1}U$: solving $\partial\hat{\boldsymbol{G}}/\partial\boldsymbol{Q}\cdot\Delta\boldsymbol{Q}=\hat{\boldsymbol{R}}$, using the numerical linearization and the $\boldsymbol{LD}^{-1}\boldsymbol{U}$ preconditioning.

5) GMRES/NumLin/P=ILU: solving $\partial\hat{\boldsymbol{G}}/\partial\boldsymbol{Q}\cdot\Delta\boldsymbol{Q}=\hat{\boldsymbol{R}}$, using the numerical linearization and the well-known incomplete $\boldsymbol{LU}$ factorization with no fill-in beyond the original nonzero pattern in $\tilde{\boldsymbol{G}}'$as preconditioning.

Figure 3 shows the convergence history for different iterative solution methods. The $LD^{-1}U$ method completes four times as many time steps Δt as the other methods for a given CPU time, but due to factorization error, the rate of convergence of the residual is substantially slower than for the other solution methods. This factorization error can be corrected with the other methods. Still, a better performance is shown by the line relaxation scheme. Only GMRES

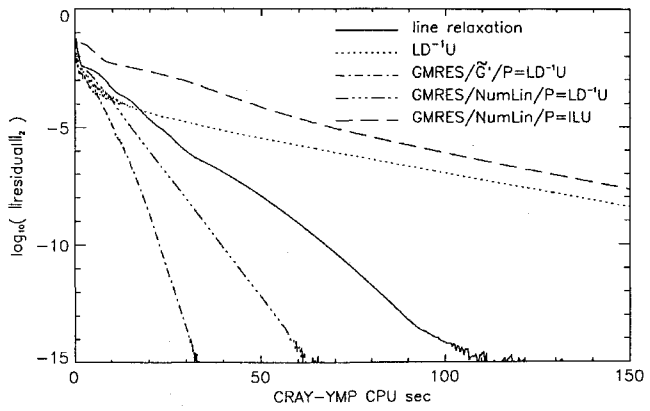

Fig. 3 Convergence history for different solution methods. Test case: laminar flow in a square cavity at $Re = 4 \times 10^2$, $\beta = 30$, and 64×64 grid points.

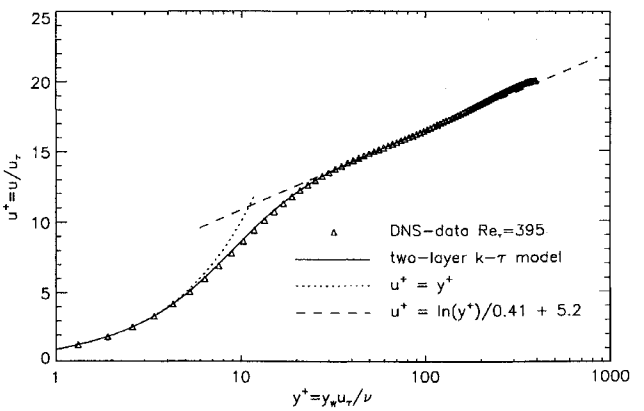

Fig. 4 Velocity distribution in the viscous sublayer and in the logarithmic layer.

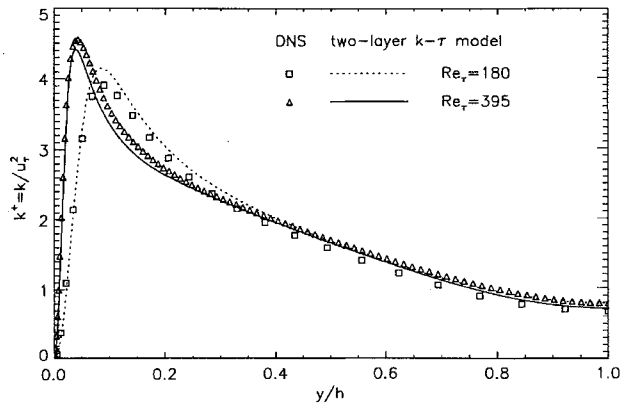

Fig. 5 Distribution of the turbulent kinetic energy between the wall and middle of the channel.

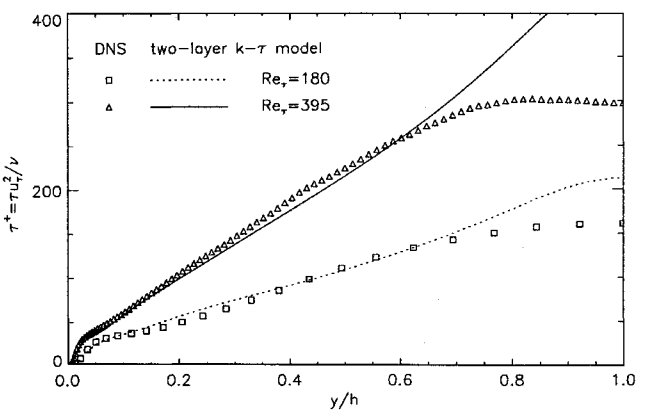

Fig. 6 Distribution of the turbulent time scale.

combined with a good preconditioner is faster. Because of the numerical linearization, the GMRES/NumLin/$P=LD^{-1}U$ is slightly slower than the solution method GMRES/$\tilde{G}'/P=LD^{-1}U$, which solves the approximate Jacobian matrix $\tilde{G}'$ directly. The influence of the preconditioning method can be seen in comparison with the GMRES/NumLin/$P=ILU$ solver. The poor vectorization properties of the recursive ILU forward and backward sweeps reduces severely the performance of this solver on a vector computer.

The laminar test case was chosen to compare different iterative solution methods. Switching to a turbulent test case, only the GMRES method combined with the numerical linearization works well and is stable to high C_S numbers [Eq. (23)]. Therefore, all of the turbulent simulations presented are computed using the GMRES/NumLin/$P=LD^{-1}U$ solution method combined with local time stepping for convergence acceleration.

Test Cases

To test and validate the two-layer k-τ turbulence model, we computed two flow configurations. First, we consider the fully turbulent channel flow at low Reynolds numbers. This test case has a simple geometry and allows us to compare the new results with the DNS data. Second, the turbulent flow over a backward-facing step is computed. This test case, with a recirculating region and a reattachment point, shows the applicability of the two-layer model to more complex flows. The computed results are compared here with experimental data.

Turbulent Channel Flow

The fully turbulent channel flow is computed for the two Reynolds numbers 1.8×10^2 and 3.95×10^2. The Reynolds number $Re_\tau = u_\tau h/\nu$ is defined using the friction velocity u_τ and the channel half-width h. For both cases, DNS data[24,25] are available and give detailed information about all turbulence quantities, especially in the wall region.

As the boundary condition on solid walls, the velocity components, the turbulent kinetic energy, the turbulent time scale, and the pressure gradient normal to the wall are set to zero. Periodic boundary conditions are used at inflow and outflow for all quantities, except for the pressure. The pressure at the inlet and outlet is fixed to match the given pressure gradient in the flow direction. Based on the integral momentum equation, the pressure gradient can be expressed as a function of the wall shear stress τ_w and combined with the friction velocity $u_\tau \equiv \sqrt{(\tau_w/\rho)}$ leads to

$$-\frac{1}{\rho}\frac{dp}{dx} = \frac{\tau_w}{\rho h} = \frac{u_\tau^2}{h} \tag{24}$$

From Eq. (24) the pressure gradient can be computed for a given Reynolds number Re_τ.

Most of the computations are performed on a 6×128 mesh with grid points clustered near the walls. Special attention is given to the near-wall resolution.

Figure 4 shows the good agreement between the two-layer turbulence model results, the DNS data, and the velocity law in the viscous and logarithmic layers. Also the turbulent kinetic energy in Fig. 5 fits the DNS data very well. Figure 6 shows the good agreement between the computations using the two-layer model and the DNS data in the wall region and also in the logarithmic layer with a near linear growth rate of the turbulent time scale. This behavior was to be expected because the algebraic model for the turbulent time scale was optimized with the aid of the DNS data for $Re_\tau = 3.95 \times 10^2$. The turbulent time scale in the middle of the channel is predicted too high. However, this has only little effect on the turbulent kinetic energy and the velocity profile. Even if the near-wall modeling of the turbulent kinetic energy and the turbulent time scale is quite good, it is difficult to match the DNS data of the turbulent dissipation rate in the viscous sublayer. This behavior can clearly be seen in Fig. 7.

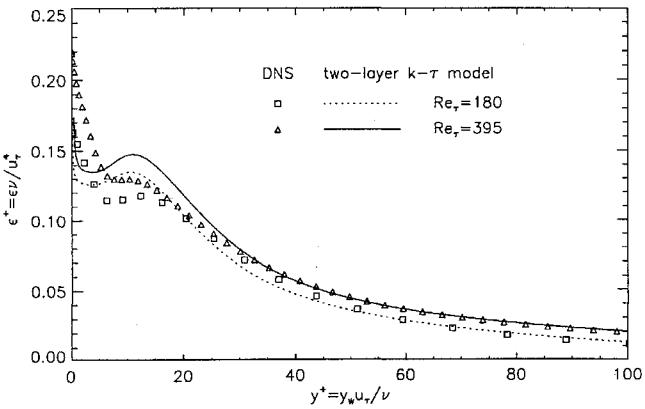

Fig. 7 Near-wall distribution of the turbulent dissipation rate.

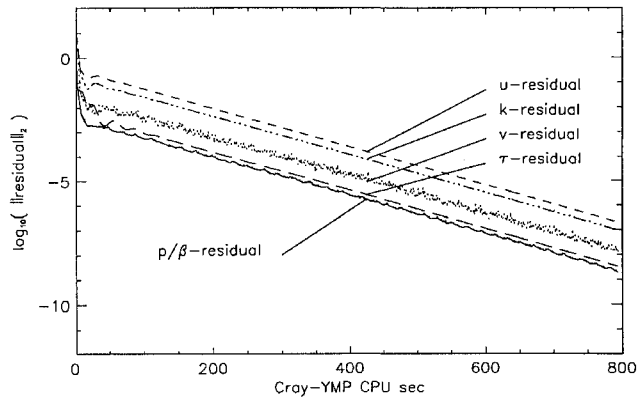

Fig. 8 Convergence history for relevant quantities on a 63 × 63 grid.

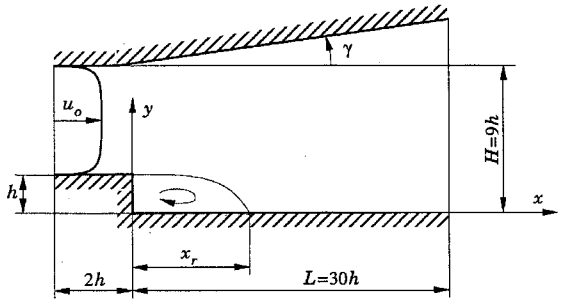

Fig. 9 Sketch of the backward-facing step channel.

To test the grid independence of the results, the computations are repeated with different numbers of grid points between the channel walls. For the turbulent channel flow test case it was found that for the turbulent kinetic energy 128 grid points or more between the channel walls are necessary for an error less than 1%. In other words, for an accuracy of 1%, a minimum of 10 grid points below $y^+ = 20$ are necessary. This is no problem for this simple test case. But for industrial flows, at high Reynolds numbers and with corresponding thin-wall layers, this leads to the requirement of highly stretched grids.

Figure 8 shows the convergence history for all relevant quantities on a 63 × 63 grid with $C_S = 100$ and $\beta = 40$. The convergence for this simple flow with optimal boundary conditions is quite good.

Turbulent Flow over a Backward-Facing Step

The turbulent flow over a backward-facing step at high Reynolds numbers was investigated in experiments by Driver and Seegmiller.[26] Based on the reference velocity $u_0 = 44.2$ m/s, the channel height $H = 0.114$ m, and the kinematic viscosity $\nu = 1.5 \times 10^{-5}$ m^2/s, the Reynolds number was $Re = 3.35 \times 10^5$ (see Fig. 9). The ratio between the channel height and the step height was $H/h = 9$. At the channel inlet the velocity profile had a boundary-layer thickness $\delta = 1.5h$ and the Reynolds number based on the momentum thickness was $Re_\Theta = 5 \times 10^3$.

With these data, inlet profiles have been generated that will be used as boundary conditions for the computations. For the horizontal velocity u, Reichardt's[29] law is used inside the boundary layer and the reference velocity in the bulk of the flow,

$$u^+ = \frac{u}{u\tau} = \mathrm{MIN}\begin{Bmatrix} u_0/u_\tau \\ \dfrac{1}{\kappa}\ell n\left(1+\kappa y_w^+\right) + 7.5\left[1 - e^{-0.1y_w^+} - 0.1y_w^+ e^{-y_w^+/3.6}\right] \end{Bmatrix}$$

with the normal distance $y_w^+ = y_w u_\tau/\nu$ measured from the wall. By matching the correct boundary-layer thickness δ and the Reynolds number Re_Θ the friction velocity is estimated to be $u_\tau = 1.805$ m/s. The turbulent kinetic energy $k^+ = k/u_\tau^2$ near the wall is computed from the following empirical equation:

$$\left[\frac{1}{k^+}\right]^2 \approx \left[\frac{1}{0.1u^{+2}}\right]^2 + \left[\frac{\sqrt{C_\mu}\tanh\left(y_w^+/30.8\right)}{1 - \left(\partial u^+/\partial y_w^+\right) - \left(y_w/\delta\right)}\right]^2$$

Between the wall layers, the turbulent kinetic energy is limited corresponding to a turbulence intensity of $Tu = 0.02$. With this value the turbulent kinetic energy in the main flow can be computed from $k = 1.5(Tu \cdot u_0)^2$.

The turbulent time scale τ can be computed from Eq. (1). Furthermore the second derivative of the pressure in the flow direction is set to zero at the inflow station. At the outflow boundary, only the pressure is specified. All other quantities are computed directly from the Navier–Stokes equations (5), neglecting the diffusive terms in the flow direction. The outflow boundary conditions are specified at 30 step heights h downstream of the step corner. On all walls, the velocity components, the turbulent kinetic energy, the time scale, and the pressure gradient in the wall normal direction are set to zero.

Driver and Seegmiller[26] presented measurements for two channel configurations. First, the parallel-wall case ($\gamma = 0$ deg) and, second, a deflected top-wall case ($\gamma = 6$ deg). The second case with its adverse pressure-gradient conditions resulted in a 30% increase in reattachment length x_r. The top-wall geometry is specified by

$$\frac{y_{\mathrm{top}}}{h} = 9 + \mathrm{MAX}\begin{Bmatrix} 0 \\ \tan(\gamma)[(x/h) + 0.47] \end{Bmatrix}$$

For the computations a mesh with 163 × 127 grid points was used. At the walls the grid is strongly stretched in the normal direction.

Figure 10 shows the streamlines just downstream of the step corner for the deflected top-wall case ($\gamma = 6$ deg). Plotting specific isolines, there is a small second recirculation visible in the lower left corner. This feature can also be seen in the experimental data. Table 2 shows a comparison of the recirculation length x_r for different computations and the experimental data. The computations presented by Driver and Seegmiller[26] were performed by Sindir and Launder. They used a standard and a modified version of the high-Reynolds-number k-ε model and the algebraic-stress turbulence model (ASM) with wall functions. In Table 2 only the results from the modified turbulence model versions are presented. Thangam et al.[12] used an anisotropic version of the low-Reynolds-number k-τ turbulence model with nonlinear corrections added to the eddy-viscosity model

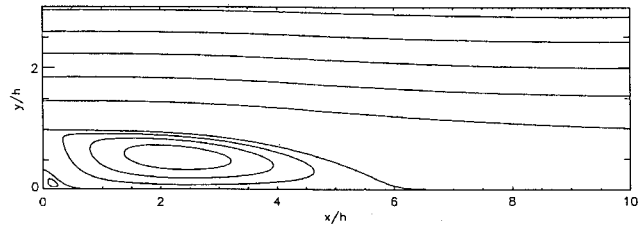

Fig. 10 Streamlines of the flow downstream of the step for the deflected top-wall case (nonequidistant isoline levels).

Table 2 Comparison of the reattachment length x_r/h for different computations with the experiments of Driver and Seegmiller[26]

γ, deg	Ref. 26	k-τ 2L[a]	k-ε^{mod} (Ref. 26)	ASM^{mod} (Ref. 26)	k-τ nl[12]	k-ε 2L[31]	k-ω[32]
0	6.1	5.7	4.6	5.8	6.0	5.5	6.4
6	8.2	6.8	5.2	7.0	——	——	8.45

[a]The present two-layer k-τ turbulence model.

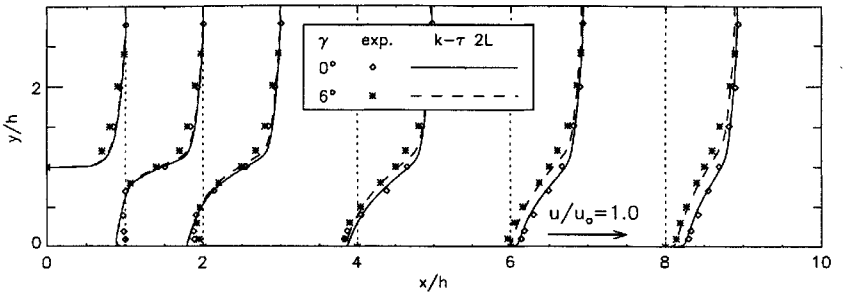

a) Mean velocity profiles

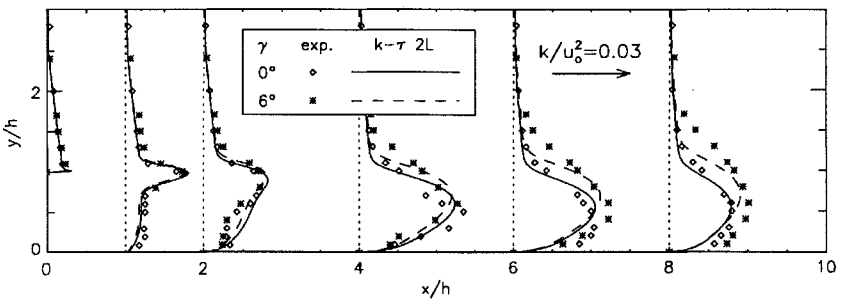

b) Turbulent kinetic energy profiles

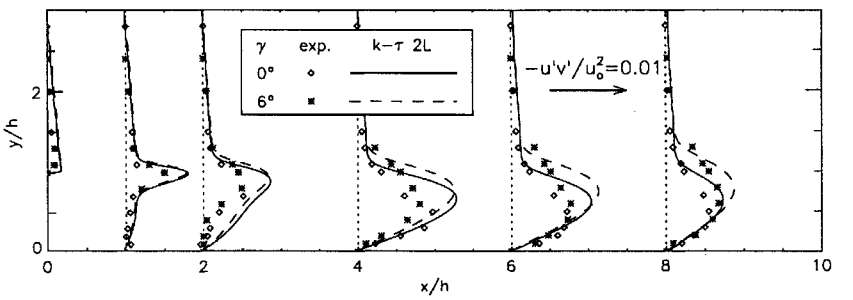

c) Reynolds stress profiles

Fig. 11 Results obtained from the two-layer k-τ turbulence model compared with the experimental data of Driver and Seegmiller[26] for the parallel-wall case ($\gamma = 0$ deg) and the deflected top-wall case ($\gamma = 6$ deg).

as developed by Speziale.[30] Also included is a two-layer k-ε computation done by Orth.[31] Additionally, results of the standard k-ω model by Wilcox,[32] which predicts the reattachment length well, are presented. In general, the two-layer model gives better results than the standard k-ε turbulence model with wall functions, but the new two-layer model still underestimates the recirculating length in the case of an adverse pressure gradient.

Profiles of the mean velocity, turbulent kinetic energy, and Reynolds stress at different x locations behind the step corner are plotted in Fig. 11. Even if the mean velocity in the recirculation region is overestimated, the overall agreement with the experimental data is good for the parallel-wall and the deflected top-wall cases. By contrast, the value of the turbulent kinetic energy for the deflected top-wall case is underestimated outside the recirculation region. A similar behavior can be seen in the Reynolds stress profiles.

Achieving a steady state in this simulation was a major problem. As starting conditions we used a laminar computation at a low Reynolds number and generated appropriate values for the turbulent kinetic energy and the turbulent time scale. Based on these values the turbulent simulation could be started with a stability parameter of $C_S \approx 1$ [Eq. (23)]. After a few time steps the parameter was increased to $C_S \approx 50$. The highly stretched grids and the complex flow configuration behind the outside corner prohibits higher C_S numbers. This has the disadvantage of a slower convergence. Especially in the near-wall region, the flow changes very slowly but still influences the main flow. Therefore, the stationarity of the calculated reattachment point must be checked very carefully. Several CPU hours are required to reach the steady state with a residual of approximately 10^{-4} at the end.

Conclusions

The robustness of the low-Reynolds-number k-τ turbulence model can be enhanced substantially by the two-layer method. With this approach, the transport equation for the turbulent time scale τ is substituted by a new algebraic equation in the vicinity of walls. The equation for the turbulent kinetic energy k is used for the whole flowfield. Therefore, only the turbulent time scale has to be matched in the wall layer by a blending function. The new algebraic equation for τ and the new damping function f_μ for the eddy viscosity in the near-wall region have been derived by using DNS data for the plane channel flow with asymptotic analysis of near-wall turbulence.

GMRES combined with the numerical linearization turns out to be a good implicit solution technique to solve the nonlinear systems of equations. The convergence of this technique can be improved substantially by the $LD^{-1}U$ preconditioning. In general, the numerical linearization allows large time steps toward the desired steady state. The solver is very suitable for vectorization and demonstrates high performance on a vector computer. A disadvantage is the problem of using a limiter for the turbulent quantities during the solution procedure inside GMRES to avoid negative values of k and τ. This leads to a limitation of the time step in the transient phase.

The new two-layer k-τ turbulence model has been applied to two test cases. The first case is the fully turbulent channel flow, computed at two low Reynolds numbers. Good agreement is found between the two-layer k-τ model results and the DNS data for both Reynolds numbers even in the viscous sublayer. The second test case is the flow over a backward-facing step computed at a high Reynolds number and with two different channel configurations. In comparison with the experimental data, the recirculating length is underestimated by 7% for the parallel-wall case and by 15% for the deflected top-wall case. This is substantially better than comparable two-equation models, but it shows once more the sensitivity of turbulence models in adverse pressure gradients.

In general, low-Reynolds-number turbulence models require a very fine grid in the normal direction near the wall. At least 10 grid points below $y^+ = 20$ are necessary for a computation with an overall accuracy of 1%. This implies strongly stretched grids and long CPU times are required to converge to the steady state. Therefore, a good solution technique and an optimal treatment of the wall layer are key features to speed up the convergence of turbulent flow simulations. In future research, special attention will be given to improved near-wall models and to further validation with DNS data of more complex flows at higher Reynolds numbers.

Acknowledgment

This work was partially supported by the Swiss National Science Foundation under Contract 21-27456.89.

References

[1]Chorin, A. J., "Numerical Method for Solving Incompressible Viscous Flow Problems," *Journal of Computational Physics*, Vol. 2, 1967, pp. 12–26.

[2]Rogers, S. E., and Kwak, D., "Upwind Differencing Scheme for the Time-Accurate Incompressible Navier–Stokes Equations," *AIAA Journal*, Vol. 28, No. 2, 1990, pp. 253–262.

[3]Patel, C., Rodi, W., and Scheuerer, G., "Turbulence Models for Near-Wall and Low Reynolds Number Flows: A Review," *AIAA Journal*, Vol. 23, No. 9, 1985, pp. 1308–1319.

[4]Speziale, C. G., Abid, R., and Anderson, E. C., "Critical Evaluation of Two-Equation Models for Near-Wall Turbulence," *AIAA Journal*, Vol. 30, No. 2, 1992, pp. 324–331.

[5]Rodi, W., and Mansour, N. N., "Low Reynolds Number k-ε Modelling with the Aid of Direct Simulation Data," *Journal of Fluid Mechanics*, Vol. 250, 1993, pp. 509–529.

[6]Rodi, W., and Mansour, N. N., "One-Equation Near-Wall Turbulence Modeling with the Aid of Direct Simulation Data," *Proceedings of the Summer Program 1990*, Center for Turbulence Research, Stanford, CA, 1990, pp. 107–124.

[7]Michelassi, V., and Shih, T.-H., "Low Reynolds Number Two-Equation Modeling of Turbulent Flows," NASA TM-104368, ICOMP-91-06, 1991.

[8]Mansour, N. N., Kim, J., and Moin, P., "Near-Wall k-ε Turbulence Modeling," *AIAA Journal*, Vol. 27, No. 8, 1989, pp. 1068–1073.

[9]Rodi, W., and Scheuerer, G., "Scrutinizing the k-ε Turbulence Model Under Adverse Pressure Gradient Conditions," *Journal of Fluids Engineering*, Vol. 108, 1986, pp. 174–179.

[10]Wilcox, D. C., "Comparison of Two-Equation Turbulence Models for Boundary Layers with Pressure Gradient," *AIAA Journal*, Vol. 31, No. 8, 1993, pp. 1414–1421.

[11]Menter, F. R., "Two-Equation Eddy-Viscosity Turbulence Models for Engineering Applications," *AIAA Journal*, Vol. 32, No. 8, 1994, pp. 1598–1605.

[12]Thangam, S., Abid, R., and Speziale, C. G., "Application of a New Model to Near-Wall Turbulent Flows," *AIAA Journal*, Vol. 30, No. 2, 1992, pp. 552–554.

[13]Norris, L. H., and Reynolds, W. C., "Turbulent Channel Flow with a Moving Wavy Boundary," Dept. of Mechanical Engineering, Stanford Univ., Rept. FM-10, Stanford, CA, 1975.

[14]Rodi, W., "Experience with Two-Layer Models Combining the k-ε Model with a One-Equation Model Near the Wall," AIAA Paper 91-0216, 1991.

[15]Cordes, J., "Entwicklung und Anwendung eines Zweischichten-Turbulenzmodells für abgelöste dreidimensionale Strömungen," Ph.D. Thesis, Univ. of Karlsruhe, Germany, 1991.

[16]Saad, Y., and Schultz, M., "GMRES: A Generalized Minimal Residual Algorithm for Solving Nonsymmetric Linear Systems," *SIAM Journal of Scientific Statistical Computation*, Vol. 7, No. 3, 1986, pp. 856–869.

[17]Brown, P. N., "A Local Convergence Theory for Combined Inexact-Newton/Finite-Difference Projection Methods," *SIAM Journal of Numerical Analysis*, Vol. 24, No. 2, 1987, pp. 410–434.

[18]Brown, P. N., and Saad, Y., "Hybrid Krylov Methods for Nonlinear Systems of Equations," *SIAM Journal of Scientific Statistical Computation*, Vol. 11, No. 3, 1990, pp. 450–481.

[19]Ajmani, K., Ng, W.-F., and Liou, M.-S., "Preconditioned Conjugate-Gradient Methods for Low-Speed Flow Calculations," NASA TM-105929, ICOMP-92-22, 1993.

[20]Venkatakrishnan, V., and Mavriplis, D. J., "Implicit Solvers for Unstructured Meshes," AIAA Paper 91-1537, 1991.

[21]Yoon, S., and Jameson, A., "Lower-Upper Symmetric-Gauss-Seidel Method for the Euler and Navier–Stokes Equations," *AIAA Journal*, Vol. 26, No. 9, 1988, pp. 1025, 1026.

[22]Yoon, S., Kwak, D., and Chang, L., "LU-SGS for Three-Dimensional Incompressible Navier–Stokes Equations with Source Term," AIAA Paper 89-1964, 1989.

[23]Yoon, S., and Kwak, D., "Three-Dimensional Incompressible Navier–Stokes Solver Using Lower-Upper Symmetric-Gauss-Seidel Algorithm," *AIAA Journal*, Vol. 29, No. 6, 1991, pp. 874, 875.

[24]Hirschberg, S., "Direkte Simulation der turbulenten Taylor-Couette Strömung und der ebenen Kanalströmung," Ph.D. Thesis, Swiss Federal Inst. of Technology, ETH Nr. 9912, Zürich, Switzerland, 1992.

[25]Shih, T.-H., and Lumley, J. L., "Kolmogorov Behavior of Near-Wall Turbulence and Its Application in Turbulence Modeling," NASA TM-105663, ICOMP-92-06, 1992.

[26]Driver, D. M., and Seegmiller, H. L., "Features of a Reattaching Turbulent Shear Layer in Divergent Channel Flow," *AIAA Journal*, Vol. 23, No. 2, 1985, pp. 163–171.

[27]Rai, M. M., "Navier–Stokes Simulation of Blade-Vortex Interaction Using High-Order Accurate Upwind Schemes," AIAA Paper 87-0543, 1987.

[28]Küffer, J., "Berechnung turbulenter Strömungen mittels Zweischicht-Turbulenzmodell," Ph.D. Thesis, Swiss Federal Inst. of Technology, ETH Nr. 10999, Zürich, Switzerland, 1995.

[29]Reichardt, H., "Die Wärmeübertragung in turbulenten Reibungsschichten," *ZAMM*, Vol. 20, 1940, pp. 297–328.

[30]Speziale, C. G., "On Nonlinear k-l and k-ε Models of Turbulence," *Journal of Fluid Mechanics*, Vol. 178, 1987, pp. 459–475.

[31]Orth, A., "Mehrgittermethode zur Berechnung inkompressibler, stationärer Strömungen mit krummlinigen Berandungen," Ph.D. Thesis, Univ. of Karlsruhe, Germany, 1991.

[32]Wilcox, D. C., *Turbulence Modeling for CFD*, DCW Industries Inc., CA, 1993, p. 161.